DOI 10.5012/bkcs.2010.31.12.3668

Electrocatalytic Reduction of Hydrogen Peroxide on Silver Nanoparticles Stabilized by Amine Grafted Mesoporous SBA-15

Mari Vinoba,[†,‡] Soon Kwan Jeong,[‡] Margandan Bhagiyalakshmi,[§] and Muthukaruppan Alagar[†,*]

[†]*Department of Chemical Engineering, Anna University-Chennai, Chennai 600025, India.* [*]*E-mail: mkalagar@yahoo.com*
[‡]*Korea Institute of Energy Research, Daejeon 305-343, Korea*
[§]*Chemical Engineering Department, Hanseo University, Seosan 360-706, Korea*
Received June 30, 2010, Accepted October 9, 2010

Mesoporous SBA-15 was synthesized using tetraethylorthosilicate (TEOS) as the silica source and Pluronic (P123) as the structure-directing agent. The defective Si-OH groups present in SBA-15 were successively grafted with 3-chloropropyl-trimethoxysilane (CPTMS) followed by tris-(2-aminoethyl) amine (TAEA) and/or tetraethylenepentamine (TEPA) for effective immobilization of silver nanoparticles. Grafting of TAEA and/or TEPA amine and immobilization of silver nanoparticles inside the channels of SBA-15 was verified by XRD, TEM, IR and BET techniques. The silver nanoparticles immobilized on TAEA and /or TEPA grafted SBA-15 was subjected for electrocatalytic reduction of hydrogen peroxide (H_2O_2). The TEPA stabilized silver nanoparticles show higher efficiency for reduction of H_2O_2 than that of TAEA, due to higher number of secondary amine groups present in TEPA. The amperometric analysis indicated that both the Ag/SBA-15/TAEA and Ag/SBA-15/TEPA modified electrodes required lower over-potential and hence possess high sensitivity towards the detection of H_2O_2. The reduction peak currents were linearly related to hydrogen peroxide concentration in the range between 3×10^{-4} M and 2.5×10^{-3} M with correlation coefficient of 0.997 and detection limit was 3×10^{-4} M.

Key Words: SBA-15, Silver nanoparticles, Amine grafting, Cyclic voltametry, Electrocatalytic reduction, Hydrogen peroxide

Introduction

Mesoporous silicas, such as MCM-41,[1] SBA-15,[2] MCM-48[3] and KIT-6[4] possess unique characteristics, various organic and inorganic compounds implanted inside their channels,[5,6] and those composite finds applications in the field of catalysis, medical[7] and sensors.[8] The functionalization of Si-OH groups in mesoporous silica with organoalkoxysilane, with specific organic groups, including amine and thiols, could immobilize and/or stabilize metal nanoparticles.[9-12] Recently, grafting of mesoporous silica with 3-chloropropyltrimethoxysilane (CPTMS) followed byother amines was recognized as a versatile route against the grafting of 3-aminopropyl trimethoxysilane, in order to plan desired number of amine groups.[13,14] In this context, the present work is proposed to synthesize mesoporous SBA-15 and grafting their Si-OH with CPTMS followed by amine grafting. The straight chain amine, tetraethylene pentamine (TEPA), and the branched amine, tris (2-aminoethyl) amine (TAEA), were chosen to graft secondary and primary amine group over chloro-functionalized mesoporous SBA-15. Furthermore, amine grafted SBA-15 was subsequently immobilized with silver nanoparticles and then subjected for electrocatalytic reduction of hydrogen peroxide (H_2O_2).

In recent times, detection of hydrogen peroxide is crucial in metal-hydrogen peroxide semi fuel cell,[15] direct methanol-hydrogen peroxide fuel cell[16] and direct borohydride-hydrogen peroxide fuel cell[17] since its reduction rate determines performance of fuel cells. Up to now, humpty numbers of methods are reported for electrocatalytic reduction of H_2O_2, for instance, spectrometry,[18] fluorimetry[19] and electrochemistry.[20] Particularly, noble metals, including Pt,[21] Pd,[22] Au,[23] Ag[24] and a combination of them, electro catalytically reduce H_2O_2 both in acidic and basic medium. The previous report on metal immobilized amine grafted mesoporous silica for the detection of H_2O_2[25] provoked us to use other amines for metal immobilization and/or stabilization for H_2O_2 reduction.

Despite the concentration of amine groups, the nature of amine group (primary or secondary) also decides the effective stabilization of the metal nanoparticles. This work presents the study of effect of primary and secondary amine for stabilization of silver nanoparticles. TEPA having three secondary amino groups and TAEA having three primary amino groups were selected for immobilization and/or stabilization of silver nanoparticles and their electro catalytic activity for reduction of H_2O_2 was studied on cyclic voltametry.

To our knowledge, no reports are available on the silver nanoparticles stabilized by TAEA/TEPA grafted mesoporous SBA-15 for electrocatalytic reduction of H_2O_2. In the present study TEPA, grafted SBA-15 effectively stabilizes the silver nanoparticles, due to the presence of three secondary amine. Even though TAEA possess three primary amino groups, stabilization of the silver nanoparticles is comparatively less than that of TEPA. TEM results and electrocatalytic reduction of H_2O_2 revealed that the nature of amine groups also play a vital role in stabilization of metal nanoparticles.

Materials and Methods

Materials. Tetraethylorthosilicate (TEOS), EO20-PO70-EO20 (Pluronic P123), 3-chloropropyl-trimethoxy-silane

(CPTMS), tris (2-aminoethyl) amine (TAEA) and tetraethylene pentamine (TEPA), silver nitrate, 37% hydrochloric acid (HCl) and indium doped tin oxide (ITO) were purchased from Aldrich and were used as received. Indium doped tin oxide after fabrication act as the electrode. Millipore water was used throughout the experiments.

Synthesis methods of SBA-15, 3-CPTMS grafting by TAEA/TEPA. SBA-15 was synthesized using a tri-block copolymer, Pluronic P123, by the reported procedure.[2] In a typical synthesis, 5 g of P123 in 190 mL of 1.6 M HCl was stirred for 1 h, and then 11.4 g of TEOS was added to the solution with vigorous stirring for 10 min. The resultant mixture was aged for 24 h at 308 K and subsequently heated for 24 h at 373 K. The solid product obtained was filtered, washed with water and ethanol, dried overnight at 373 K, and finally calcined at 823 K for 4 h.

50 mM of CPTMS was added to 1 g of SBA-15 dispersed in 70 mL of dry toluene under vigorous stirring. Then the mixture was refluxed at 353 K for 24 h and the final product was filtered, washed with toluene followed by alcohol and dried under vacuum at 343 K for 8 h. The product was denoted as SBA-15/CPTMS.[13] 1 mmol of amine compounds (TAEA / TEPA) was subsequent graftedon 1 g SBA-15/CPTMS by same procedure. Thereafter the products were named as SBA-15/X Amine (where X Amine is TAEA and TEPA). [13]

Immobilization of silver nanoparticles over the SBA-15/TAEA or TEPAand preparation of modified electrode. 100 mg of SBA-15/TAEA or TEPA was dispersed in 10 mL of 0.1 mmol $AgNO_3$ was added, the mixture was stirred at room temperature for 4 h and then vaccum dried. The solid sample obtained was washed with minimum amount deionized water to remove the excess silver nitrate on external surface of SBA-15/TAEA or TEPA.[26] Then, controlled reduction of $AgNO_3$ was done by drop wise addition of $NaBH_4$ solution and continued stirring for another 24 h. Finally, the solid product was filtered, washed, dried under vacuum at 333 K.[26] The products are denoted as Ag/SBA-15/TAEA and Ag/SBA-15/TEPA. Scheme 1 represents the grafting of TAEA/TEPA on SBA-15 followed by the immobilization of silver nanoparticles.

The fabrication of the Ag/SBA-15/TAEA or TEPA/ITO modified electrodes is summarized as follows: ITO glass plate of geometric area 1cm^2 and R = 15 Ω/cm^2 was cleaned by sonicating sequentially for 5 min each in acetone and millipore water and finally washed with copious amount of millipore water. Ultrasonic dispersion of 1 mg of Ag/SBA-15/TAEA or TEPA in 1 mL of alcoholic APTMS solution gives a yellow suspension of 1.0 mg/mL. Subsequently, 4 μL of this yellow suspension was dropped onto the surface of the cleaned ITO electrode and allowed to dry at ambient temperature. These modified electrodes thereby denoted as Ag/SBA-15/TAEA/ITO and Ag/SBA-15/TEPA/ITO.

Characterization. Powder X-ray diffraction patterns were recorded using a Rigaku Miniflex diffractometer with Cu-Kα radiation (λ = 0.154 nm). The diffraction data were recorded in the 2 θ range of 0.5 - 10° at 0.02° step size and 1 s step time. The nitrogen adsorption-desorption isotherms were measured at 77 K on a Micromeritics ASAP 2010 volumetric adsorption

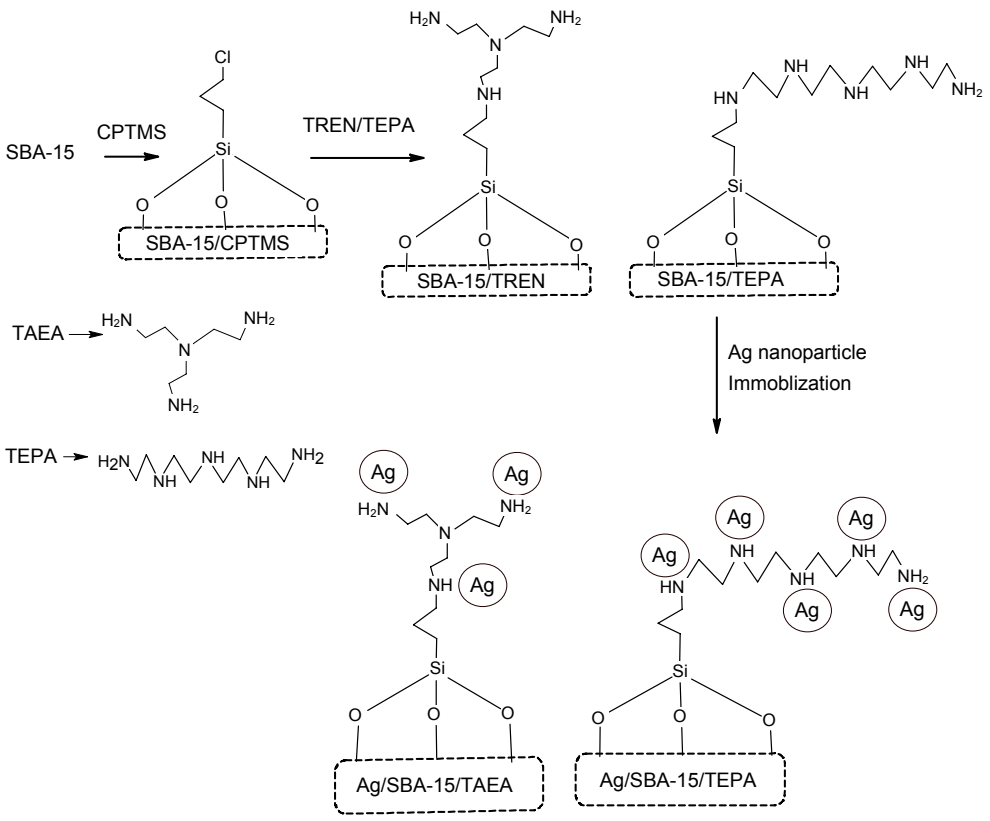

Scheme 1. Schematic of TAEA and TEPA grafting on chlorofunctionalized mesoporous silica and subsequent silver nanoparticle immobilization

analyzer. Prior to each adsorption measurement the samples were evacuated at 378 K under vacuum for 4 h in the degas port of the adsorption analyzer. The specific surface area (S_{BET}) was determined from the linear part of BET equation and the pore size using the Barrett-Joyner-Halenda (BJH) method. Fourier Transform Infrared (FTIR) spectra of the samples were recorded at room temperature on a Nicolet 6700 spectrometer equipped with an ATR (attenuated total reflection) cell. Each sample was scanned twenty times at 4 cm^{-1} resolution over the range 4000 ~ 400 cm^{-1}. HR-TEM and EDX analysis were performed on JEOL-2000EX electron microscope operating at the accelerating voltage of 120 kV. Proton-decoupled ^{29}Si MAS NMR spectra were recorded on a JEOL (JNM-LA400WB) 400 MHz spectrometer at 79.4 MHz with a sample spinning frequency of 5 KHz. Elemental analysis was done by FISONS EA-1108 analyser.

Electrochemical studies. Cyclic voltametric and amperometric measurements were performed on CHI modal 1100A series electro chemical analyzer (CH Instrument, USA). Ag/SBA-15/TAEA or TEPA fabricated ITO plate acts as working electrode with Pt foil (large surface area) and a saturated calomel electrode (SCE) as counter and reference electrodes, respectively. Then the electrode was cleaned by cycling between the potentials of −0.2 and + 1.5 V *versus* SCE in 1 M H_2SO_4 at a scan rate of 100 mV s^{-1} for approximately 30 min until reproducible scans were recorded. All the electrochemical experiments were performed in a quiescent solution at room temperature.

Results and Discussion

Characterization. Fig. 1. shows the XRD patterns of parent SBA-15, SBA-15/TAEA or TEPA and Ag/SBA-15/TAEA or TEPA. The XRD patterns show well ordered hexagonal mesophase for parent SBA-15, while SBA-15/CPTMS, SBA-15/TAEA or TEPA and Ag/SBA-15/TAEA or TEPA show no significant change or shift in XRD peaks position. There observed only decrease in intensity of peaks, which was reported to be the function of scattering contrast between silica walls and pore channel, perhaps due to pore filling by CPTMS followed by TAEA/TEPA grafting.[27,28] Furthermore, disappearance and/or absence of the higher order (hkl) peaks of SBA-15/CPTMS, SBA-15/TAEA or TEPA and Ag/SBA-15/TAEA or TEPA depicts, pore filling and/or successive structural construction of CPTMS and TAEA/TEPA and the silver nanoparticles.

N_2 adsorption-desorption isotherms of the parent SBA-15 SBA-15/TAEA or TEPA and Ag/SBA-15/TAEA or TEPA are presented in Fig. 2. The surface area of all the materials was evaluated using BET method, the pore size by BJH method (isotherms with hysteresis). Their textural properties are summarized in Table 1. The nitrogen adsorption/desorption of pristine SBA-15 (3A) shows type IV isotherm with a sharp step up in a narrow range of relative pressure (P/Po = 0.68 - 0.75) arising from the capillary condensation of nitrogen in the mesopores. The pore volume of SBA-15 is large enough to accommodate the TAEA and/or TEPA in addition to the silver nanoparticles. Therefore, even after grafting and immobilization with TAEA/TEPA and silver nanoparticles, the mesoporosity of SBA-15 is retained.[28]

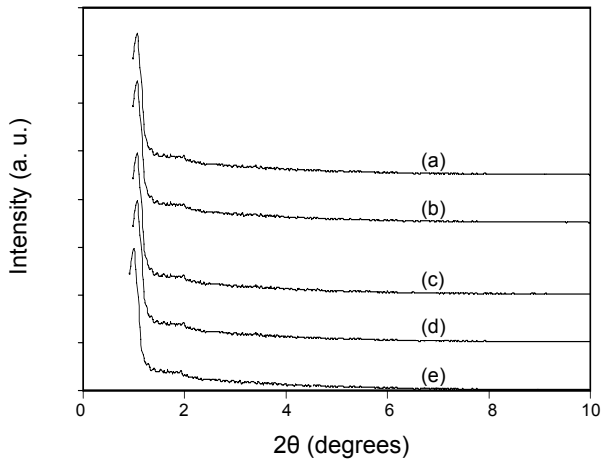

Figure 1. XRD pattern for (a) SBA-15; (b) SBA-15/TEPA; (c) SBA-15/TAEA; (d) Ag/SBA-15/TEPA; e) Ag/SBA-15/TAEA.

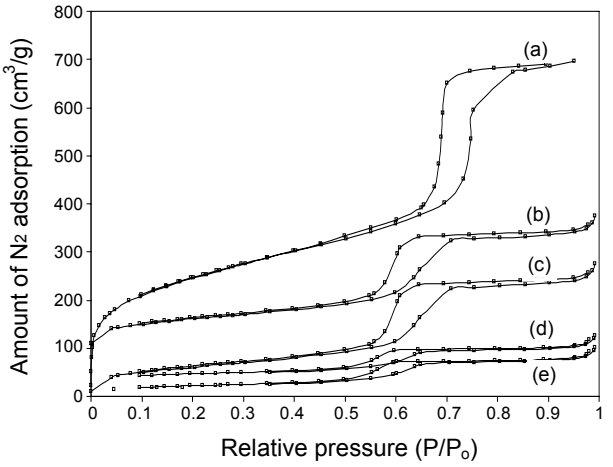

Figure 2. The N_2 adsorption-desorption isotherm of (a) SBA-15; (b) SBA-15/TEPA; (c) SBA-15/TAEA; (d) Ag/SBA-15/TEPA; (e) Ag/SBA-15/TAEA.

Table 1. Textural properties of Ag/SBA-15/TAEA and Ag/SBA-15/TEPA

Materials	S_{BET} (m^2/g)	V_p (cm^3/g)	D_p (nm)
SBA-15	834.2	0.88	6.20
SBA-15/CPTMS	516.2	0.53	4.56
SBA-15/TAEA	202.3	0.23	3.59
SBA-15/TEPA	212.4	0.28	3.65
Ag/SBA-15/TAEA	103.4	0.11	3.20
Ag/SBA-15/TEPA	109.3	0.10	3.34

*S_{BET} - specific surface area; V_p - total pore volume; D_p - pore diameter

Fig. 3. illustrates FTIR spectra of the parent SBA-15, SBA-15/TAEA, SBA-15/TEPA, Ag/SBA-15/TAEA and Ag/SBA-15/TEPA. The IR spectra of SBA-15/TAEA and SBA-15/TEPA shows band at 1465 cm^{-1} due to -CH_2 scissoring vibrations of alkyl group present in TAEA and TEPA. The bands in the region 1515 - 1558 cm^{-1} are attributed to asymmetric and symmetric

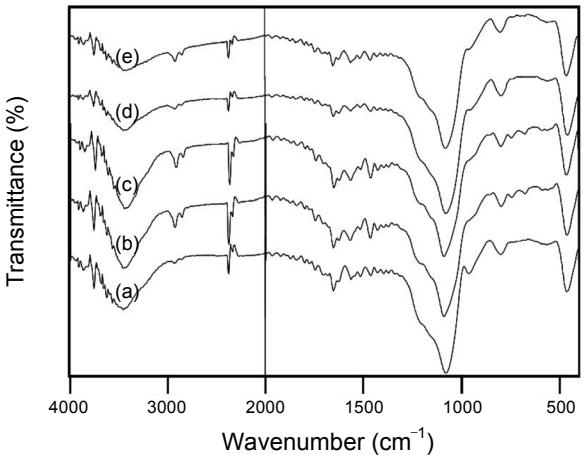

Figure 3. IR spectrum of (a) SBA-15; (b) SBA-15/TEPA; (c) SBA-15/TAEA; (d) Ag/SBA-15/TEPA; (e) Ag/SBA-15/TAEA.

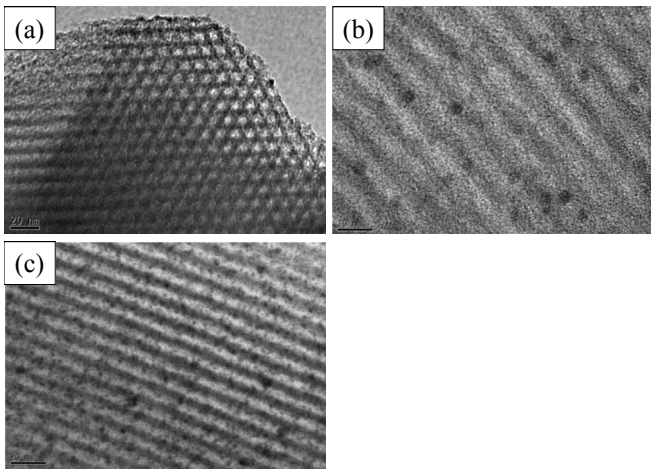

Figure 4. TEM images of (a) SBA-15; (b) Ag/SBA-15/TEPA; (c) Ag/SBA-15/TAEA.

bending vibrations of the primary amine groups respectively. Furthermore, the reaction between defective Si-OH group and CPTMS is clearly evidenced by decrease in intensity of bending absorption band at around 960 cm^{-1} and appearance of new bands at 3307 and 3378 cm^{-1} are due to -NH_2 vibrations in SBA-15/TAEA, SBA-15/TEPA. The shift in the absorption bands of the primary amino groups to higher wave number in Ag/SBA-15/TAEA and Ag/SBA-15/TEPA evidences the stabilization of silver atoms by amine groups present in SBA-15/TAEA, SBA-15/TEPA.[29]

The microscopic features of the parent SBA-15, Ag/SBA-15/TAEA and Ag/SBA-15/TEPA were captured by high-resolution transmission electron microscope (HRTEM) are shown in Fig. 4. The TEM image of parent SBA-15 shows hexagonally arranged mesopores while the dark spots in Ag/SBA-15/TAEA and Ag/SBA-15/TEPA represents the stabilization of silver nanoparticles inside the hexagonal mesopores of SBA-15/TAEA and SBA-15/TEPA with size ranging from 1 - 3 nm. From the TEM images, dark spots representing silver nanoparticles are comparatively more in Ag/SBA-15/TEPA than that of Ag/SBA-15/TAEA. Silver nanoparticles are immobilized by stronger reducing ability of secondary amine while primary amine associates with the particle surface due to the electrostatic interaction between the positively charged amine groups and aggregates over it.[30] Therefore, the silver nanoparticles are highly stabilized by secondary amine compared to primary amine. As the electrochemical reduction of hydrogen peroxide is proportional to amount of silver atoms on the surface of the electrode, Ag/SBA-15/TEPA material shows slightly higher sensitivity towards

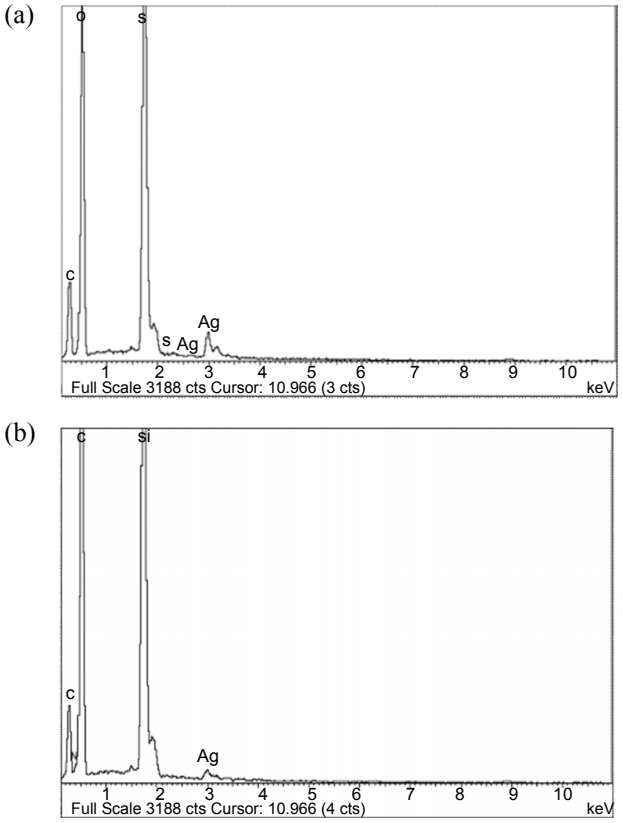

Figure 5. EDX spectrum of (a) Ag/SBA-15/TEPA; (b) Ag/SBA-15/TAEA.

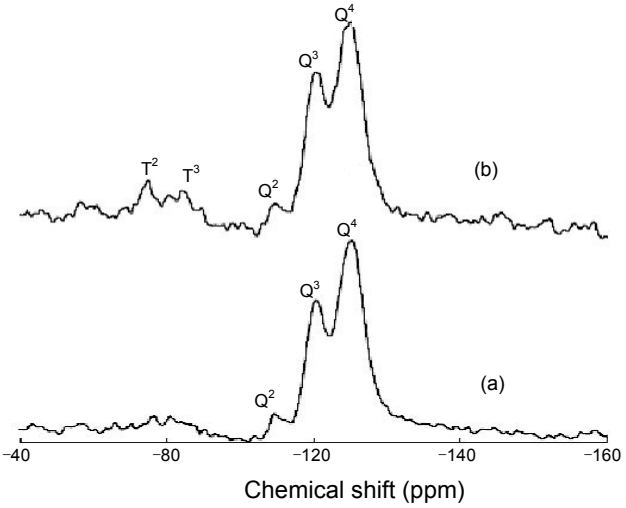

Figure 6. ^{29}Si MAS NMR of (a) SBA-15; (b) SBA-15/CPTMS.

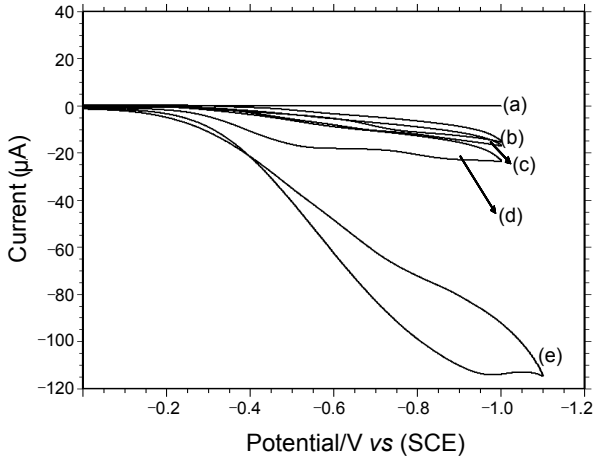

Figure 7. Electrocatalytic reduction of hydrogen peroxide upon modified with 2 mM H_2O_2 (a) Bare ITO; (b) ITO/Ag; (c) ITO/APTES/Ag; (d) Ag/SBA-15/TERN; (e) Ag/SBA-15/TEPA

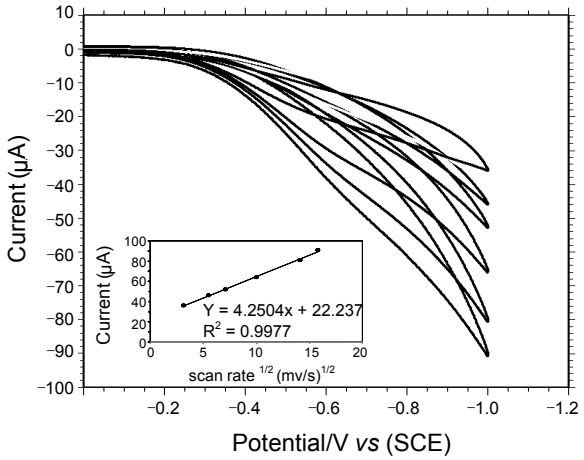

Figure 8. Cyclic voltammetric response of Ag/SBA-15/TEPA in pH 7 PBS at scan rates (inner to outer) 10, 30, 50, 100, 200, and 250 mVs^{-1}. Inset, plot of peak current Vs. $v^{1/2}$.

H_2O_2 reduction than that of Ag/SBA-15/TAEA and proved to be true by the electrochemical analysis.

The amount of TEPA and TAEA grafted over SBA-15 were quantified by elemental analysis, the nitrogen content and amine concentration for SBA-15/TAEA and SBA-15/ TEPA is 5.6 and 5.4 wt % and 1.51 and 1.40 mmol/g, respectively. EDX analysis of Ag/SBA-15/TAEA and Ag/SBA-15/ TEPA confirms the presence of Ag (Fig. 5). The Ag content in Ag/SBA-15/TAEA and Ag/SBA-15/ TEPA are 4.86 and 4.94 wt % respectively.

Fig. 6. depicts ^{29}Si-MAS-NMR of parent SBA-15 and SBA-15/CPTMS. The two peaks at −101.3 and −109.3 ppm are attributed to Q^3 ($Si(OSi)_3(OH)$) and Q^4 ($Si(OSi)_4$) silicon atoms, respectively (Fig. 6a). The co-condensation of CPTMS over SBA-15 showed the T^2 ($Si(OSi)R(OH)$) as well as T^3 ($Si(OSi)R$) peak signals (Fig. 6b) at −74 and −77 ppm respectively, indicating that two and three free silanols are involved during reaction between defective Si-OH groups of mesoporous silica and CPTMS.[13]

Electrocatalytic reduction of hydrogen peroxide on Ag/SBA-15/TAEA and Ag/SBA-15/TEPA modified electrodes: Fig. 7 displays the electrocatalytic reduction of hydrogen peroxide on Ag/SBA-15/TAEA and Ag/SBA-15/TEPA working electrode by cyclic voltametry. The electrochemical response of Ag/SBA-15/TEPA in the selective phosphate buffer solution (PBS) in the pH range 5.0 to 8.0 dictates no significant effect. Therefore, the neutral pH 7.0 was set as the optimum pH value for electrocatalytic reduction of hydrogen peroxide. Fig. 7(d) and 7(e) illustrates the electrocatalytic reduction of 2 mM H_2O_2 on Ag/SBA-15/TAEA and Ag/SBA-15/TEPA working electrode in pH 7.0 PBS. The CV of bare ITO electrode and ITO/Ag shows no reduction peaks, which indicates that there was no reduction of H_2O_2 in the solution while CV of Ag/SBA-15/TAEA and Ag/SBA-15/TEPA shows small reduction current. Silver nanoparticles stabilized on the amine groups attribute to such electrocatalytic reduction of H_2O_2 on Ag/SBA-15/TAEA and Ag/SBA-15/TEPA. Pervious reports on the oxidation of H_2O_2upon several modified electrodes depicted relatively high over potential (e.g., 0.7 V *vs*. SCE at Pt electrode), which makes the electrode sensitive to interferences from many electro active species such as ascorbic acid and uric acid.[31] In the present study, the silver nanoparticles stabilized on both Ag/SBA-15/TEPA and Ag/SBA-15/TAEA play similar role in increasing or decreasing the over potential. Furthermore, the nature of amine compound either secondary or primary amine present in the TAEA and TEPA influences the reduction current. Thereafter with Ag/SBA-15/TEPA, the enhanced reduction peak current starting at about −0.45 V implies a typical electrocatalytic reduction process of H_2O_2. This suggests a faster electron transfer rate and higher electrocatalytic activity towards the reduction of H_2O_2 with Ag/SBA-15/TEPA by the effect of silver nanoparticles stabilized by the secondary amine of TEPA. In case of Ag/SBA-15/TAEA, the electrocatalytic reduction occurs at slightly lower activity due to well-dispersed silver nanoparticles on branched TAEA amine. The decomposition of H_2O_2 by silver-catalyst is similar to the reported mechanism [32] as represented in the equations 1 and 2.

$$H_2O_2 \xrightarrow{Ag} \frac{1}{2}O_2 + H_2O \quad (1)$$

$$O_2 + 2e^- + 2H^+ \xrightarrow{ITO} H_2O_2 \quad (2)$$

Hydrodynamic amperometric study of Ag/SBA-15/TEPA modified electrode. The effect of applied potential on the steady-state current of the Ag/SBA-15/TEPA was studied at the potential ranging from −0.2 V to −1.0 V and the results are displayed in Fig. 8. The amperometric response for the reduction of H_2O_2 at −0.4 V shows that steady state current increases with the negative shift of the potentials and reaches a plateau at −0.6 V. Therefore, amperometric detection of H_2O_2 was carried out at −0.4 V to decrease or avoidthe interferences caused by some electro active species lower working potential.

Fig. 9A illustrates the typical amperometric *I-t* curve of Ag/SBA-15/TEPA working electrode at −0.4 V on the successive

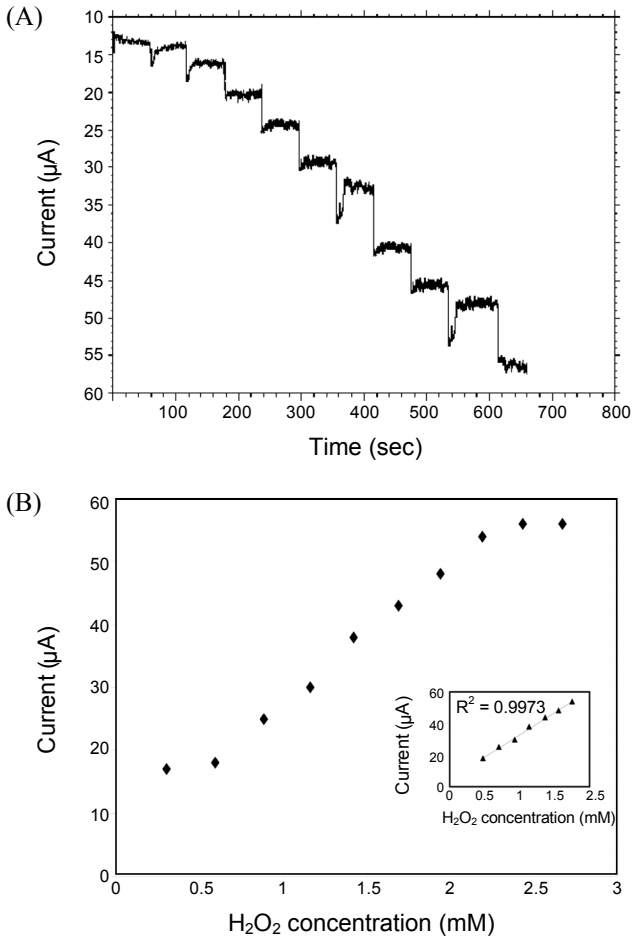

Figure 9. (A) Amperometric response of Ag/SBA-15/TEPA potential was held at −0.4 V in buffer solution (pH 7) for successive addition 2 mM H_2O_2. (B) Calibration plot between the steady-state current and H_2O_2 concentration. Inset is plot between the steady-state current and H_2O_2 concentration obtained from the upper limit of the linear range.

addition of H_2O_2 into N_2-saturated PBS (pH 7.0). On H_2O_2 addition into the stirring buffer solution, the sensor responded rapidly to reach a steady state. The sensor could achieve 95% of the steady-state current within 5s, which is in agreement with earlier report.[25] The Ag/SBA-15/TEPA displayed a wider linear range from 3×10^{-4} M to 2.5×10^{-3} M with a correlation coefficient of 0.997 and a slope of 22.44 μA (Fig. 9B). The detection limit of 3×10^{-4} M (Fig. 9B) is lower than those obtained with the reported peroxidase - based H_2O_2 sensors[24] and silver nanoparticle - GCE. This wider linear range and higher sensitivity depicted by the Ag/SBA-15/TEPA film on the electrode surface and its respective electrocatalytic activity might be due to the dispersion as well as the stabilization of SBA-15/TEPA. The amine compounds stabilize the nanosize silver particles inside the channel of SBA-15; hence, metal leaching was restricted, despite larger pore diameter of SBA-15. Therefore, such intact silver nanoparticles rules out the environmental contamination concerned with leaching. Thus, the results obtained indicate the direct detection of H_2O_2 with Ag/SBA-15/TEPA.

When Ag/SBA-15/TEPA working electrode is stored in air and subjected to day-by-day calibrations at room temperature, the electrode can maintain over 97% of the initial value in response to 2.0 mM H_2O_2 after 100 days, during electrochemical reduction of H_2O_2. Therefore, this Ag/SBA-15/TEPA is both reproducible and stable while the bulk silver electrode decayed quickly to 92% after 24 hours.

Conclusion

In this study, mesoporous SBA-15 was successfully grafted the straight chain TEPA and branched TAEA amines and subsequently immobilized with silver nanoparticles. N_2 adsorption/desorption and TEM studies evidences that large pore of SBA-15 could comfortably host both the TAEA and/or TEPA and silver nanoparticles. Their electrocatalytic activity was studied by the reduction of hydrogen peroxide. Preliminary tests of both the Ag/SBA-15/TAEA and Ag/SBA-15/TEPA exhibited a high electrocatalytic activity to the reduction of hydrogen peroxide. Ag/SBA-15/TEPA possesses higher activity than that of Ag/SBA-15/TAEA, due to the stabilizing efficiency of secondary amine (TEPA) than that of primary amine (TAEA).

Acknowledgments. This research was supported by a grant (CK3-101-1-0-0) from Carbon Dioxide Reduction & Sequestration Research Center, one of the 21st Century Frontier Programs funded by the Ministry of Education Science and Technology of Korean government.

Reference

1. Kresge, C. T.; Leonowicz, M. E.; Roth, W. J.; Vartuli, J. C.; Beck, J. S. *Nature* **1992**, *359*, 710.
2. Zhao, D.; Feng, J.; Huo, Q.; Melosh, N.; Fredrickson, G. H.; Chmelka, B. F.; Stucky, G. D. *Science* **1998**, *279*, 548.
3. Xu, J.; Luan, Z.; He, H.; Zhou, W.; Kevan, L. *Chem. Mater.* **1998**, *10*, 3690.
4. Kim, T. W.; Kleitz, F.; Paul, B.; Ryoo, R. *J. Am. Chem. Soc.* **2005**, *127*, 7601.
5. Liu, X.; Wang, A.; Yang, X.; Zhang, T.; Mou, C. Y.; Su, D. S.; Li, J. *Chem. Mater.* **2009**, *21*, 410.
6. Zhu, J.; Knya, Z.; Puntes, V. F.; Kiricsi, I.; Miao, C. X.; Ager, J. W.; Alivisatos, A. P. *Langmuir* **2003**, *19*, 4396.
7. Rosenholm, J. M.; Lindén, M. *J. Controlled Release* **2008**, *128*, 157.
8. Liu, Y.; Zhang, J.; Hou, W.; Zhu, J. *J. Nanotechnology* **2008**, *19*, 135707.
9. Vinu, A.; Hossain, K. Z.; Ariga, K. *J. Nanosci. Nanotechnol.* **2005**, *5*, 347.
10. Walcarius, A.; Etienne, M.; Lebeau, B. *Chem. Mater.* **2000**, *15*, 2161.
11. Walcarius, A.; Etienne, M.; Sayen, S.; Lebeau, B. *Electroanalysis* **2003**, *15*, 414.
12. Wan, Y.; Zhang, D.; Hao, N.; Zhao, D. *Int. J. Nanotechnol.* **2007**, *4*, 66.
13. Bhagiyalakshmi, M.; Yun, L. J.; Anuradha, R.; Jang, H. T. *J. Hazard. Mater.* **2010**, *175*, 928.
14. Brunel, D. *Micropor. Mesopor. Mater.* **1999**, *27*, 329.
15. Yang, W.; Yang, S.; Sun, W.; Sun, G.; Xin, Q. *Electrochim. Acta* **2006**, *52*, 9.
16. Prater, D. N.; Rusek, J. J. *Appl. Energy* **2003**, *74*, 135.
17. Miley, G. H.; Luo, N.; Mather, J.; Burton, R.; Hawkins, G.; Gu, L.; Byrd, E.; Gimlin, R.; Shrestha, P. J.; Benavides, G.; Laystrom, J.; Carroll, D. *J. Power Sources* **2007**, *165*, 509.
18. Matsubara, C.; Kawamoto, N.; Takamura, K. *Analyst* **1992**, *117*,

1781.
19. Li, J.; Dasgupta, P. K. *Anal. Chem.* **2000**, *72*, 5338.
20. Song, Y.; Wang, L.; Ren, C.; Zhua, G.; Li, Z. *Sensor Actuat B-Chem*. **2006**, *114*, 1001.
21. vanVenrooij, T. G. J.; Koper, M. T. M. *Electrochim. Acta* **1995**, *40*, 1689.
22. Yang, W.; Yang, S.; Sun, W.; Sun, G.; Xin, Q. *Electrochim. Acta* **2006**, *52*, 9.
23. Strbac, S.; Adzic, R. R. *J. Electroanal. Chem.* **1992**, *337*, 355.
24. Flatgen, G.; Wasle, S.; Lubke, M.; Eickes, C.; Radhakrishnan, G.; Ertl, G. *Electrochim. Acta* **1999**, *44*, 4499.
25. Lin, D. H.; Jiang, Y. X.; Wang, Y. *J. Nanomater.* **2008**, 473791.
26. Zhao, Y.; Qi, Y.; Wei, Y.; Zhang, Y.; Zhang, S.; Yang, Y.; Liu, Z. *Micropor. Mesopor. Mater*. **2008**, 111, 300.
27. Kim, S.; Ida, J.; Guliants, V. V.; Lin, J. Y. S. *J. Phys. Chem. B* **2005**, *109*, 6287.
28. Neimark, A. V.; Ravikovitch, P. I.; Grün, M.; Schüth, F.; Unger, K. K. *J. Colloid Interface Sci.* **1998**, *207*, 159.
29. Selvaraj, V.; Alagar, M. *J. Bionanoscience* **2008**, *2*, 54.
30. Wang, S. T.; Yan, J. C. *Mater. Lett.* **2005**, *59*, 1383.
31. Delvaux, M.; Walcarius, A.; Demoustier-Champagne, S. *Anal. Chim. Acta* **2004**, *525*, 221.
32. Pirault-Roy, L.; Kappenstein, C.; Guerin, M.; Eloirdi, R. *J. Propulsion Power* **2002**, *18*, 1235.